Proceedings World Geothermal Congress 2015
Melbourne, Australia, 19-25 April 2015

On the Impact of Spatial Permeability Heterogeneity on the Characteristic Wavelength of Free Convection Cells in the Perth Basin, Australia

Jan Niederau[1], Anozie Ebigbo[1], Sebastian Freitag[2], Gabriele Marquart[1], Bernd Hentschel[2] and Christoph Clauser[1]

[1] Institute for Applied Geophysics and Geothermal Energy, E.ON Energy Research Center, RWTH Aachen University, Germany

[2] Virtual Reality Group, RWTH Aachen University, Germany

jniederau@eonerc.rwth-aachen.de

Keywords: free convection, numerical modelling, permeability heterogeneity, correlation length, Perth Basin, Australia

ABSTRACT

When dealing with free convection in a geothermal reservoir, it is preferable to detect regions of up flow, which locally increase the geothermal gradient. Free convection cells are likely to be found in a large reservoir layer (Yarragadee Aquifer), which is encountered in the entire Perth Basin, including the Perth Metropolitan Area (PMA). While the knowledge about the structure of the Perth Basin has been improved recently, the heterogeneity and spatial complexity of permeability was up till now mainly neglected.

We set up a refined structural model of about 5000 km² comprising the region around the city of Perth up to a depth of 4.5 km, using an implicit modelling approach (3D GeoModeller by Intrepid Geophysics). Based on the structural model we create a discretized numerical model for simulating fluid flow and heat transport in the Yarragadee Aquifer considering spatial heterogeneity of porosity and permeability. This heterogeneity is assessed by designing three different test cases: 1) constant porosity and permeability for the entire aquifer; 2) porosity and permeability decreasing with depth; 3) a conditional random permeability field within prescribed limits and for given correlation length.

We calibrate a poro-perm relationship based on a fractal approach to the Yarragadee Aquifer, using over 100 measurement pairs of porosity and permeability from three boreholes. This data was also used for calibrating porosity decrease with depth, following Athy's law.

For the model with constant porosity and permeability, convection cells vary in size between 4 km and 6 km. Simulations with depth dependent decrease in porosity and permeability yielded a transition from conductive to convective heat transport in the Yarragadee Aquifer at a threshold permeability of around 1.7×10^{-15} m². There convection cells are much smaller, at the scale of 2.4 km to 3 km. Stochastic distributions of porosity and permeability in the Yarragadee cause the formation of convection cells to adjust to the permeability field, yielding a less distinct convection pattern.

Where the Yarragadee Aquifer is in contact with overlying aquifers, stable regions of down flow develop. These in turn have a strong impact on the regional flow field and therefore on the temperature distribution. Temperatures drop to about 40 °C in 2 km depth.

In order to improve the reliability of the model, as well as identification and comparison of convection cells in different simulations, we are developing a specialized visualization tool tailored to this purpose. By using tools like particle tracing and direct volume rendering, the recognition of the spatial distribution of convection cells and their change in the different cases facilitated.

1. INTRODUCTION

The city of Perth was rated among the TOP 10 geothermal cities worldwide (GEA, 2009). This may not only be attributed to the geologic setting of the Perth Basin, but also to the potential for direct heat use, as a major part of the electric energy demand is consumed by air conditioning (63% for an average Australian household, according to the Australian government). As the majority of chiller systems (compression chillers) require electric energy to function, technologies for direct-heat use are desirable. Sorption chillers may fit in this niche, although their energy efficiency is low compared to compression chillers. This, however, may be misleading. Efficiency turns in favor of sorption chillers, taking into account that compression chillers are operated using electricity (i.e. fossil fuels). Thus, sorption chillers are advantageous when a direct-heat supply is in economic range, as it is in the case of the sedimentary Perth Basin. Major deep confined aquifers with reported high average permeability are suited for hydrothermal energy extraction. While the heat extracted from deep aquifers within the Perth Basin may not suffice to generate electricity, it allows for direct heat use (e.g. St. Hilda's school geothermal well). With the foundation of the Western Australian Geothermal Center of Excellence (WAGCoE) in 2008, the Perth Basin as a geothermal system has been subject to intensive and thorough exploration (Poulet & Corbel, 2012; Timms et al., 2012; Reid et al., 2012; Ricard et al., 2012).

Regarding the documented exploration results from hydrocarbon exploration, a major aquifer (Yarragadee Aquifer) consisting of Jurassic sedimentary successions is estimated to be suited for geothermal energy exploitation. Particularly the role of free convection within this ca. 2 km thick aquifer was considered to; on the one hand generate locally favorable conditions (i.e. regions of increased geothermal gradient), on the other hand increase uncertainty of estimated temperatures at depth. While the resolution of the structure of the Perth Basin around the Perth Metropolitan Area (PMA) was refined by the WAGCoE, the spatial heterogeneity and complexity of porosity and permeability was up till now not included in hydrothermal simulations (Schilling et al., 2013).

Within this work, we present an approach to assess the impact of spatial heterogeneous porosity and permeability on the evolution of free convection cells. In particular, how this heterogeneity influences the characteristic wavelength of free convection cells compared to aquifer structure, i.e. its thickness. For this purpose, three different case studies were designed and applied to the Yarragadee Aquifer: 1) homogeneous, yet anisotropic porosity and permeability distribution; 2) a calibrated decrease in porosity and permeability with depth; 3) a random porosity and permeability field, related by a fractal approach. Furthermore, the effect of hydraulic interconnection between different aquifer layers on the temperature field is examined and supports results published in Schilling et al. (2013).

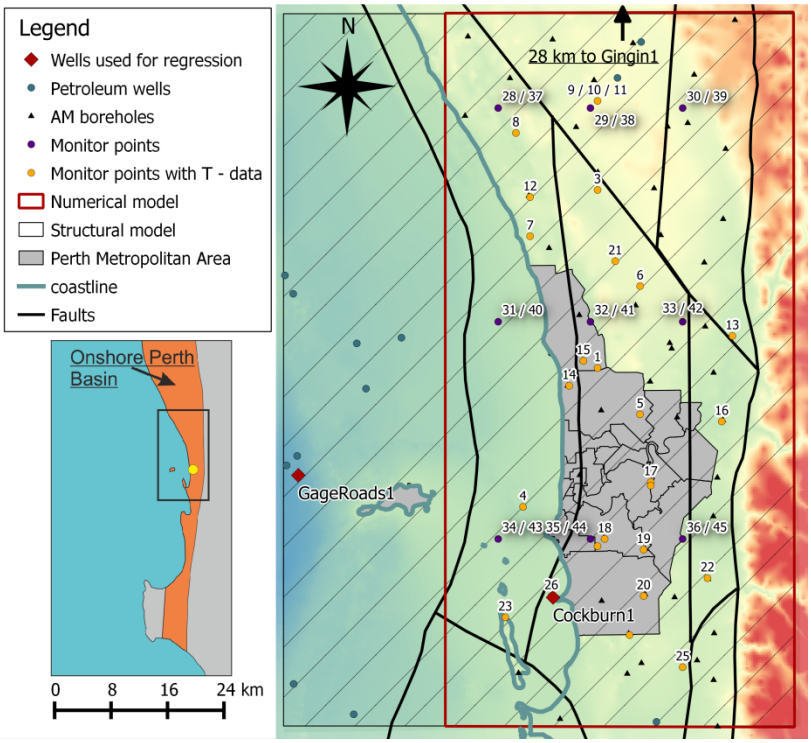

Figure 1: Location of the study area. Color coding reflects topography with red values = higher altitudes. Note that the structural map was recently refined in Timms et al. (2012) (modified from Crostella and Backhouse, 2000).

2. GEOLOGICAL MODEL

A brief knowledge about the geological setting and the setup of the structural model is crucial to understand the simulation results discussed later. This section will provide a short summary of the geological background and the generation of the structural model. Further, we present the calibration of a porosity-permeability relationship, which is valuable for generating calibrated input data for the numerical simulations.

2.1 Geological Background

The Perth Basin is a north-south elongated sedimentary trough on the south-western continental margin of Australia (Fig.1). It developed during rifting in the Permian, which concluded with the final break-up between greater India and Australia in the Cretaceous. Thus, the Perth Basin is filled with Permian to Cenozoic sediments (and subordinate and locally with volcanic rocks). The thickness of the sedimentary sequences is documented to be up to 15 km. Deep sedimentary, siliciclastic aquifers within the basin represent possible targets for geothermal energy extraction. More precisely, these are the Triassic Lesueur Sandstone and Jurassic fluviatile sediments, referred to as the Yarragadee Formation. In particular the latter is a possible target extensively analyzed in the recent years (Ricard et al., 2011; Corbel et al., 2012; Reid et al., 2012a; Sheldon et al., 2012), whereas the Perth Basin has also been subject to detailed geological studies (Playford et al., 1976; Backhouse, 1984; Iasky, 1993; Cadman et al., 1994; Crostella & Backhouse, 2000), mainly as a consequence of exploration of possible hydrocarbon resources. This is why valuable data on e.g. temperature or petrophysical parameters (e.g. thermal conductivity, porosity, permeability, radiogenic heat production) were collected and available for this study (see CSIRO, 2007). Within the scope of WAGCoE, additional data on thermal conductivity, porosity and permeability were measured (DellePiane et al., 2013) and incorporated in our work.

As stated before, the majority of lithologies encountered in the Perth Basin are of siliciclastic origin, reflecting different stages of the rifting process from the Permian to the Cretaceous. Sedimentary setting varied between continental and marine as a response to sea level changes and subsidence. As a consequence, porosity and permeability is directly dependent on facies/lithology, i.e. hydrological units (DellePiane et al., 2013). Differential extension along the main rift axis of the basin is indicated by a varying sediment thickness across the basin and the generation of transform faults, which cut through strata and older normal faults. Those normal faults previously formed a complicated graben system with several sub-basins (e.g. Vlaming sub basin) which had different subsidence rates inside the whole Perth Basin. The differential subsidence in those sub-basins ceased with the final break-up in the Cretaceous, which is marked by a basin-wide unconformity (Neocomian unconformity). This unconformity is the base of sediments, which accumulated in a transgressive milieu, such as the South Perth Shale (SPS). Directly overlying the Yarragadee Aquifer, the SPS-unit acts as a sealing layer for the Yarragadee Aquifer and separating it from the even younger Leederville

Aquifer. However, where the SPS-unit is absent, hydraulic exchange between the Yarragadee and the Leederville Aquifer is possible (Davidson & Yu, 2008; Schilling et al., 2013).

Whether a combination of conduction and advection or convection is the dominant transport mechanism in the Yarragadee aquifer is still debated (Sheldon et al., 2011; Sheldon et al., 2012 and references therein). However, significant lateral temperature differences at depth measured in the northern Perth Basin would require a significant lateral change in thermal conductivity if solely explained by conduction.

2.2 Structural Model

Information on the depth of geological formations from altogether 83 boreholes (65 shallow artesian monitoring wells and 18 deep petroleum wells) within our working area provides the basis for the structural model. As the majority of these boreholes are shallow groundwater monitoring wells, the subsurface is well resolved up to a depth of about 1000 m (Australian height datum [AHD]). In addition, the shallow groundwater system down to the Neocomian unconformity is modelled in detail within the Perth Regional Aquifer Modelling System (PRAMS) (Davidson & Yu, 2008). While these two data sources allow for a refined structural model at shallower depth, the capability of modelling hydrothermal processes within deeper aquifers is limited within PRAMS.

Using data from the 83 wells and geological data (i.e. geological cross sections and models), we set up a 3D-structural model of the Perth Basin around the City of Perth, further called Perth Metropolitan Area (PMA). Emphasis was laid on best possible modelling of the Yarragadee Aquifer, as this unit is regarded as an important geothermal target in the Perth Basin. Within the WAGCoE initiative, a refined structural model of the central Perth Basin was published by Corbel et al. (2012). Both models agree in important key features, such as local absence of the SPS and therefore hydraulic interconnection between the Leederville and Yarragadee Aquifer or the overall shape of the Yarragadee Aquifer. Similarly to the model by Corbel et al. (2012), we conflated the basin formations into aquifers and aquitards, depending on their hydraulic properties (Fig. 2). Minor shallow aquifers were resolved in the Leederville Aquifer or the Superficial Aquifer.

The structural model covers an area of 100 km (north-south) times 50 km (east-west) and extends to a depth of 4.5 km in order to include the complete Yarragadee Aquifer. In total 7 main fault systems were introduced into the model, although studies by Timms et al. (2012) suggest a significant larger number of faults. But as they are usually small, shallow and of less vertical extend, they unlikely affect the Yarragadee Aquifer. We focused on prominent faults (e.g. Darling Fault or Eneabba Fault) in the structural model because they significantly influence the geometry of the Yarragadee Aquifer. Fault nomenclature was adapted from Crostella and Backhouse (2000).

For constructing the 3D-structural model, we used an implicit potential-field modelling approach (Lajaunie et al., 1997) which is implemented in the Software package 3D-GeoModeller (e.g. Calcano et al., 2008). One main advantage is that this approach is its potential in handling sparse data coverage, as geologic contact points are seen to be on an equipotential surface, which is interpolated by the use of co-kriging.

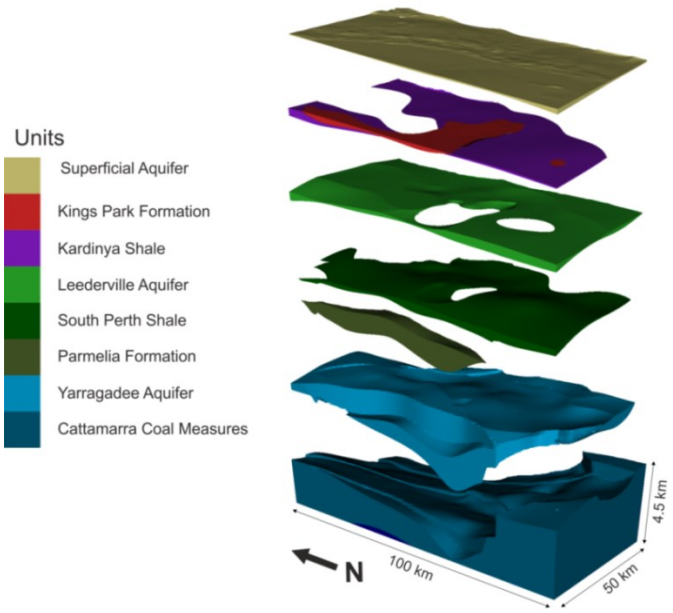

Figure 2: Stacked view of the structural model (vertical exaggeration 4:1). Note that the South Perth Shale Aquitard is not present over the whole lateral model extend, thus enabling hydraulic interaction between Yarragadee Aquifer and Leederville Aquifer.

2.3 Porosity-permeability relationship

Ehrenberg and Nadeau (2005) illustrate that reservoir rocks worldwide show a wide variability in porosity and permeability. From this variability, it can be deduced that porosity and permeability are complexly interdependent. Evolution of primary porosity and permeability with depth is not only dependent on burial and thermal exposure, but also on the original lithology. That is why

defined empirical models are usually only valid for the specific region, where the data was collected. Non-empirical models usually build up on the Kozeny-Carman equation. We use a combination of the Kozeny-Carman equation with fractal theory (Pape et al., 1999, 2000; Costa, 2006) for calibrating a porosity-permeability model (Pape et al., 1999) for the Yarragadee Aquifer.

$$k = A\phi + B\phi^{\exp 1} + C(10\phi)^{\exp 2} \tag{1}$$

where $\boldsymbol{k}$ is permeability [nm²], ϕ porosity [-] and A, B and C are coefficients to be calibrated by nonlinear regression. Ideally, also *exp1* and *exp2* should be estimated by nonlinear regression. These exponents are directly connected to the fractal dimension of the rock.

For calibration of equation (1), 104 pairs of measurements on porosity and permeability were provided by Delle Piane et al. (2013) and CSIRO (2007). The calibration is described in more detail in Niederau (2014). The resulting nonlinear regression fits acceptably with the data points, although it seems to slightly overestimate permeability in porosity ranges around 8 %. Note that the regression at lower porosities is uncertain for there is unsufficient data coverage.

$$k = 166\phi + 19904\phi^{2.8.} + 388(10\phi)^{8.01} \tag{2}$$

Equation 2 is used to relate porosity and permeability in our numerical models. In doing so, a porosity distribution with depth is derived from available sonic logs and then translated to a permeability distribution by using equation (2).

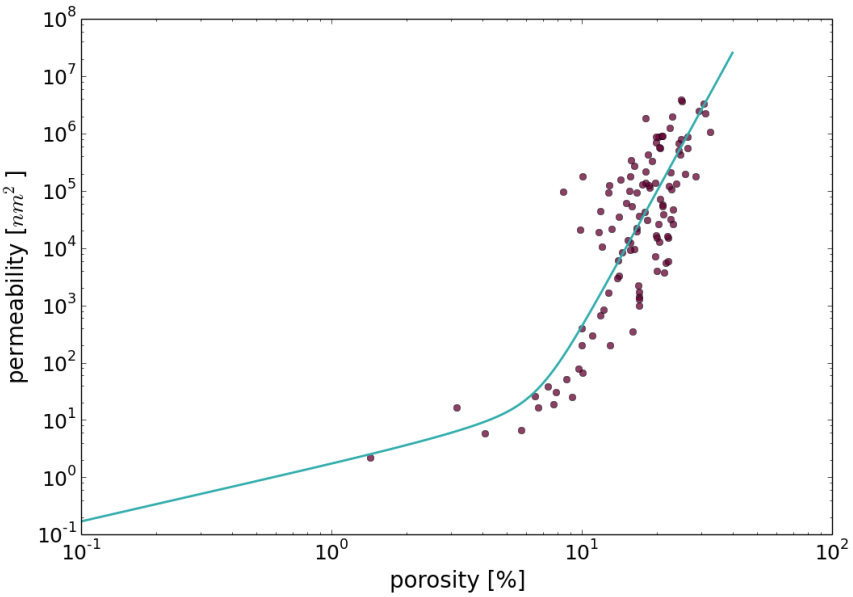

Figure 3: Nonlinear regression – equation 2 - of 104 measurements on cores, which stem from three boreholes over the Perth Basin.

The provided data further show that with increasing depth porosity decreases. As a reduced porosity / permeability influences the development of free convection cells, we explicitly consider the depth dependence of porosity in case study 2). For this purpose, a calibration of Athy's law (Athy, 1930) was introduced:

$$\phi(z) = \phi_0 e^{(-\alpha z)} \tag{3}$$

where $\boldsymbol{\phi}$ is porosity at depth $\mathbf{z}$, $\boldsymbol{\phi_0}$ the initial porosity, $\boldsymbol{\alpha}$ a correlation factor and $\mathbf{z}$ is depth [m]. Considering a wide range of porosities within the Yarragadee Aquifer, nonlinear regression yields

$$\phi(z) = 0.28e^{(-2.6\times10^{-4}z)} \tag{4}$$

As mentioned before, porosity distributions are deduced from sonic logs, as there are no additional logs available. However, these logs were used in a traditional variogram analysis to assess a vertical correlation length of porosity in respect to the grid size of our numerical model. The variogram analysis was carried out using the geostatistical library GSLIB (Deutsch and Journel, 1998) and yielded a vertical correlation length of about 90 m.

3. NUMERICAL SIMULATION

3.1 Numerical model

The structural model was exported in an equidistant grid of 97 × 200 × 97 nodes (cell size is 500 m × 500 m × 50 m) yielding a discretized model of around 1.9 million cells. An aspect ratio of 10 (horizontal to vertical) was chosen in order to resolve thin units (e.g. parts of the South Perth Shale or units above the Leederville Aquifer). Nine units in total are represented in the numerical model (table 1). Faults are represented as displacement, not as distinct units.

3.2 Equations and simulation code

Fluid and heat transport within porous media is simulated using the code SHEMAT-Suite (Rath et al., 2006), which is based on a finite-difference scheme in a 3D-Cartesian coordinate system. The transient flow equation used in our simulations is based on Darcy's law and the mass balance equation:

$$\nabla \cdot \left[\frac{\rho_w g k}{\mu_w} \left(\nabla h + \rho_r \nabla z \right) \right] + Q = S_s \frac{\partial h}{\partial t} \tag{5}$$

where $\boldsymbol{\rho_w}$ is the density of water [kg m^{-3}], $\boldsymbol{\mu_w}$ the dynamic viscosity of water [kg (m s)$^{-1}$], $\boldsymbol{g}$ gravity [m s^{-2}], $\boldsymbol{k}$ permeability [m²], $\boldsymbol{h}$ the hydraulic head [m], $\boldsymbol{z}$ the vertical coordinate in space [m], and $\boldsymbol{\rho_r} = (\rho_f - \rho_0)\ \rho_0^{-1}$ describes the relative change of water density towards a reference density ρ_0. $\boldsymbol{Q}$ is a specific flow rate [s^{-1}] and $\boldsymbol{S_s}$ the specific storage coefficient [m^{-1}].

Analogue to the flow equation emerging from the mass balance equation, the heat transport equation may be derived from Fourier's law and the energy balance equation:

$$\nabla [\lambda_e \nabla T] + (\rho c)_w v \nabla T + H = (\rho c)_e \frac{\partial T}{\partial t} \tag{6}$$

where $\boldsymbol{\lambda_e}$ is the tensor of the effective thermal conductivity [W m^{-1} K^{-1}], $\boldsymbol{T}$ temperature [°C], $\boldsymbol{(\rho c)_w}$ and $\boldsymbol{(\rho c)_e}$ are the volumetric heat capacities of water and the fluid-saturated porous medium [J m^{-3} K^{-1}], respectively. $v = \frac{\rho_w g k}{\mu_w} (\nabla h + \rho_r \nabla z)$ equals the specific discharge [m s^{-1}], $\boldsymbol{H}$ the heat generation rate [W m^{-3}].

3.3 Simulation parameters and boundary conditions

Due to the classification into aquifers and aquitards, nine different units are resolved in the numerical model. Their ascribed petrophysical parameters are shown in table 1.

Table 1: Simulation parameters. References: (A) CSIRO(2007); (B) Schilling et al. (2013); (C) HDRPL (2008); (D) Botman (2010); (E) Middleton (2013)

Units	Porosity	vert. Permeability [10^{-15} m²]	Thermal conductivity [W m^{-1} K^{-1}]	rad. heat production [µW m^{-3}]
Superficial Aquifer	0.3	118	3.4	0.2
Kings Park Formation	0.1	11.8	3.4	0.3
Kardinya Shale	0.1	0.0118	1.4	0.6
Leederville Aquifer	0.3	118	3.4	0.6
South Perth Shale	0.1	0.0118	1.8	0.82
Parmelia Formation	0.2	0.0118	3.1	0.5
Yarragadee Aquifer	1) 0.22 2) 0.08 – 0.28	1)11.8 2) 0.1 – 125	4.3	0.5
Cattamarra Coal Measures	0.1	0.0118	4.1	0.5
Basement / Yilgarn Craton	0.01	0.0012	3.2	4
References	A	B	C	D,E

For maintaining comparability with already published results (Schilling et al., 2013), we use no-flow boundary conditions on the lateral boundaries of our model in a first approach. For the eastern boundary, this is reasonable as the units of the Yilgarn Craton

are generally impermeable. The choice of the other boundaries to be closed is debatable (Schilling et al., 2013). For the top boundary of the model, we use a Dirichlet boundary condition for head, which represents the elevation of the water table / sea level. Similar to Schilling et al. (2013) temperature boundary conditions were chosen to be 20 °C for the top boundary condition and 110 °C for the bottom. On the one hand, this value is in agreement with available literature (Crostella & Backhouse, 2000), on the other hand a defined specific heat flow as a bottom boundary condition should be preferred over a fixed temperature.

Model calibration is difficult due to its highly transient behavior. Temperature measurements for deep boreholes are usually uncorrected and there is not sufficient data to apply a correction method, e.g. a Horner Plot. Albeit having a number of temperature measurements for the artesian monitor wells, they are often too shallow, as only a few reach the top of the Yarragadee Aquifer. However, in future models with a stochastic permeability field, these temperature measurements may be useful for assessing a confidence range of temperature variation at a given position in the model, i.e. position of the well where the data stems from.

As mentioned in the introduction, we set up three different cases to assess the impact of correlation length on the development of free convection cells: 1) constant porosity and permeability for the entire aquifer (infinite correlation length); 2) porosity and permeability decreasing with depth (large finite vertical correlation length); 3) a conditional random permeability field within prescribed limits (finite vertical and horizontal correlation length)

In accordance with literature data, permeability is set anisotropic ($\kappa_{vertical} = 0.1\ \kappa_{horizontal}$) in every simulated scenario.

4. VISUALIZATION

For facilitating the analysis of simulation results for knowledge acquisition and their communication, a specialized visualization application has been developed that is tailored for geothermal simulation data and the requirements at hand. In order to improve the efficient understanding of the inherently three-dimensional datasets (Billen et al., 2008; Laha et al., 2012) and enhance depth perception, an immersive Virtual Reality-based visualization approach was chosen. It is constructed upon the ViSTA Virtual Reality toolkit (Assenmacher & Kuhlen, 2008).

At its core, a direct volume rendering visualization enables the user to inspect whole three-dimensional scalar fields at once and to quickly identify salient features even in unexpected areas (Fig. 5a). It is complemented by additional classical visualization techniques including two-dimensional slices and isosurfaces. Furthermore, data can be sampled along a line and plotted (Fig. 5). For analyzing thermal highs and lows as well as for assessing their lateral distance directly, features such as sampling along a line are especially valuable.

Vector fields can be examined using interactive particle tracing. Here, the user can interactively insert massless particles or streamlines into a vector field and follow their motion to quickly and intuitively understand the three-dimensional structure of that field. Particle tracing further helps to evaluate the correctness of the regional flow field and convection pattern, thus facilitates the identification of potential error sources.

A strong focus lies on the interactivity of the visualization. For all techniques, the visualization updates live while the user changes the corresponding value. This allows, e.g., to quickly find salient isosurfaces just by sliding through the value range, to rapidly place a 2D slice at the best or most meaningful position, interactively move or rotate the line along which samples are plotted or to update the color map and visible value range based on the visibility of interesting features.

5 RESULTS

In order to mitigate early transient oscillation when convection cells form, we chose a simulation time of around 3 million years. Similar studies suggest that a dynamic steady state is reached after ca. 1 million years. In the following, the results after 3 million years for the three cases are presented.

Figure 4 shows the temperature distribution at a model depth of 1.5 km for the three different scenarios. The first scenario (Fig. 4a) shows free convection with distinct upwelling areas in the south-western part of the model. There, the Yarragadee Aquifer is about 1.9 – 2.3 km thick. Towards the south-eastern part of the model, the distinct convective pattern ceases abruptly, as the Yarragadee Aquifer gets significantly thinner. The visible change of the convective pattern can be connected to a normal fault, trending north-south (Fig. 1) and dipping towards the west. In the north-east of the model, an elongated zone of up-flow is observed adjacent to the darling fault. A big region of significantly reduced temperatures at depth is visible in the northern part of the model. This is connected to hydraulic connection between the Yarragadee Aquifer and the Leederville Aquifer. Temperatures peak at around 90 °C in the center of the upwelling area, while it decreases to 25 °C in zones of down flow.

In the scenario of depth-dependent change of porosity and permeability, a different convection pattern is encountered (Fig. 4 b). At 1.5 km depth, areas of up flow and down flow are less marked and thinner compared to case 1 and case 3. Lateral temperature variations are significantly smaller. This originates from the fact that heat transport in the second case changes from mainly conductive to convective at a threshold permeability of about 0.9×10^{-15} m², corresponding to a depth of about 2 km. That is to say, convection occurs in a thinner part of the Yarragadee Aquifer, as compared to case 1 and case 3. As a consequence, the convective cells have a smaller wavelength because temperature difference and thickness of the convective layer are less than in case 1 and 3. Regions of up-flow are significantly thinner than in case 1 and 3. Note that depth dependent decrease of permeability is unlikely to be the same all over the modelled Yarragadee Aquifer, as indicated by petrographic studies by Timms et al. (2012). That is to say, this model reflects an extreme of a possible model suite, in which differential decrease in porosity with depth could be assessed.

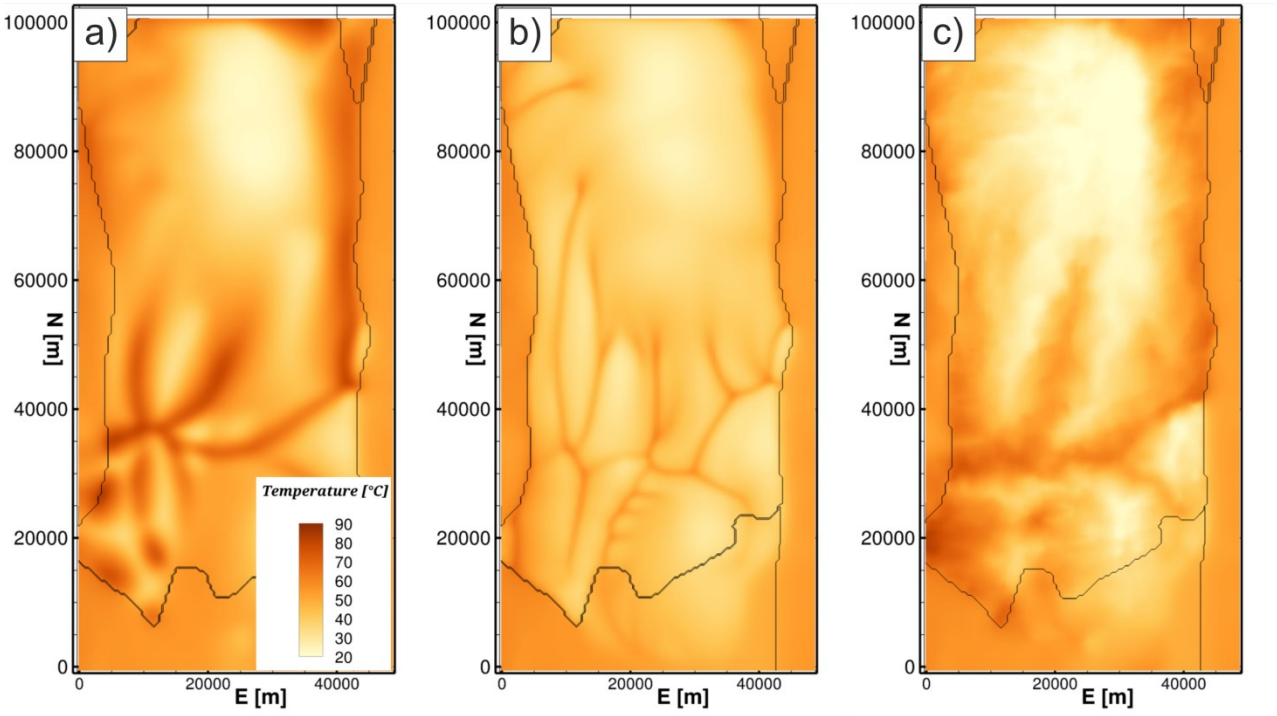

Figure 4: Horizontal slices at 1.5 km depth showing the temperature distribution after a simulation time of 3 million years. The square shows the idealized position of the Perth City Center. a) homogeneous porosity and permeability, b) decrease in porosity and permeability with depth, c) stochastic porosity and permeability field.

Case 3 (Fig. 4c) includes lateral and vertical variations of porosity and permeability, as it is expected in a sedimentary setting. As the obtained correlation length by variogram analysis is small compared to the discretized model dimensions, no striking sedimentary structures can be observed. Furthermore, this porosity and permeability field was generated stochastically, and does by no means reflect the true spatial poro-perm distribution in the Yarragadee Aquifer.

Nonetheless, spatial variations in porosity and permeability perturb the regional flow field and change the convective pattern compared to the homogeneous case (Fig. 4a and 4c). Dominant zones of upwelling can be identified in both cases in the same model domains (e.g. south-west or north-east). This can be attributed to the structure of the Yarragadee aquifer, whose thickness is maximal in the south-west (2.3 km) and in the north-east (2.7 km). As stated before, upwelling areas can often be linked to structural features, i.e. fault displacement. Yet, the implementation of finite correlation lengths for porosity and permeability has a significant effect on the shape of convective cells and the convection pattern. Borders of convection cells are not as distinct as in case 1 and there are less individual zones of upwelling in the south-west.

Regions of decreased temperatures are found in the north of all three modelled scenarios (Fig. 4, 5). The SPS, which acts as a barrier to flow and a sealing layer for the Yarragadee Aquifer, thins out towards the north-east and is absent in the north of our structural model (Fig. 2). There, the Yarragadee Aquifer is in direct contact with the shallower Leederville Aquifer, allowing for hydraulic exchange. Where the two aquifers are connected, stable regions of down flow develop. Apart from the absence of a flow barrier, one driving factor, which enables the development of these stable regions of down flow, is the higher groundwater table in the north-east of the model (Fig. 1). Due to the resulting difference in hydraulic head, water flows towards south in the Leederville Aquifer and enters the Yarragadee Aquifer where they connect, creating a region of down flow. The descending cold water creates a zone of decreased temperatures at depth in the Yarragadee Aquifer in the north of the model (Fig. 5).

This becomes more evident when using the possibilities of visualization. Figure 5 shows the temperature distributions for all three scenarios along a horizontal north-south trending line at a depth of around 2.4 km. To properly adjust the line, temperatures were blanked above 90 °C and below 50 °C in the 3D-Model (Fig. 5a). In a moveable graph, values of a desired property (here temperature, y-axis) are plotted according to their position on the line (x-axis). Plotting occurs simultaneously as the sampling line is moved, enabling a fast and intuitive assessment of the model.

Significant temperature drops are recorded along the line in each of the three scenarios. In case 1 and 3, temperature drops locally below 30 °C in case 3. Note that the temperature difference in case 2 is way smaller than in case 1 and 3, due to the fact that heat conduction is dominant in deeper parts of the Yarragadee Aquifer. The observation of temperature anomalies connected to hydraulic exchange between the Aquifers is supported by comparable studies (Schilling et al., 2013).

As a consequence, the structural model, especially when discretized into a numerical grid, has to be as accurate as possible in order to prevent the generation of unwanted short circuits between the Aquifers. That is why we chose a fine discretization in the vertical direction.

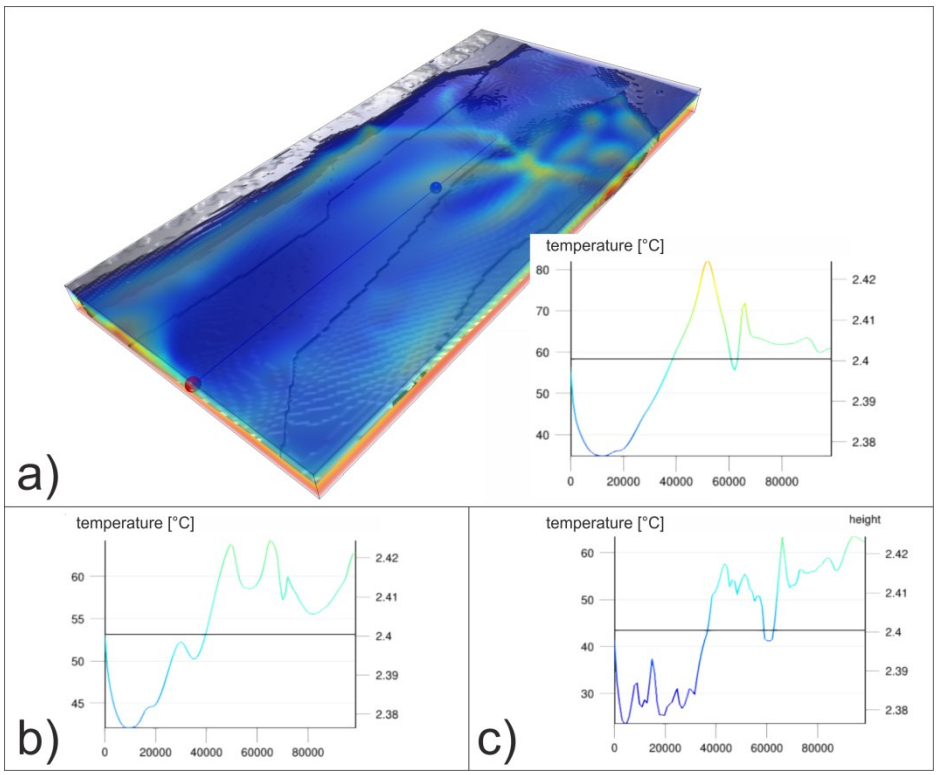

Figure 5: Assessment of lateral temperature variations along a north-south trending line. a) homogeneous porosity and permeability. The graph displays the temperature along the line visible in the 3D model. b) graph showing the temperature at the same position for the second case, c) same for the scenario with a stochastic permeability field. Measurements were done in an immersive visualization software (section 4). The second y-axis marks inclination of the line, which is horizontal in our measurements (black line).

6. CONCLUSION

In order to assess the impact of spatial heterogeneous permeability on the generation of convective cells and their size / wavelength, we generated three different test cases, which stem from the same structural model.

Simulation results show that correlation length has a significant impact on the shape and to a lesser extent, on the position of convective cells. While the spatial location of an upwelling area is also influenced by the thickness of the aquifer, its shape is influenced by anisotropy and heterogeneity of permeability. Decrease in porosity and permeability with depth show a transition from conductive to convective heat transport at a permeability of about 0.9×10^{-15} m².

Compared to the homogeneous, anisotropic case 1, the implementation of a stochastic permeability field showed that individual convection cells are not well evolved, but rather merge and coalesce as a consequence of pathways, which in turn are generated by spatial heterogeneous permeability. However, regions of upwelling seem to be primary be controlled by the reservoir structure. Where the Yarragadee Aquifer and Leederville Aquifer are connected, regions of down flow develop, which in turn have a strong impact on the lateral temperature distribution, generating a region of reduced temperatures connected to regions of down flow. Thus, minimizing the uncertainty of the geological model is of primary importance for ensuring meaningful simulation results.

As temperatures in our simulations vary between 25 °C and 90 °C at 1.5 km depth, possible borehole locations have to be chosen with care. While our models are unlikely to represent the true temperature regime in the PMA, the results give meaningful indications as to why the consideration of heterogeneous permeability is important for geothermal reservoir simulations. Temperature measurements from shallow artesian monitor wells may be used for calibration of the hydrothermal models. However, due to the complexity and transient behavior of the system, these temperature measurements should more be considered as a quality control of the simulation results. The successful calibration of a fractal porosity-permeability relationship provides a possibility to extract valuable information about permeability from porosity, which can normally be deduced from well-logs.

ACKNOWLEDGEMENTS

This study is part of the MeProRisk-II project, funded by the Federal Ministry of Environment (grant 0325389).

REFERENCES

Assenmacher, I. and Kuhlen, T: The ViSTA Virtual Reality Toolkit. In Software Engineering and Architectures for Realtime Interactive Systems (SEARIS), 23–26, (2008).

Billen, M. I., Kreylos, O., Hamann, B., Jadamec, M. A., Kellogg, L. H., Staadt, O., and Sumner, D. Y: A Geoscience Perspective on Immersive 3D Gridded Data Visualization. Computers & Geosciences, 34(9), 1056-1072, (2008).

Botman, C.: Determining the geothermal properties of the Perth Basin lithology to aid geothermal energy projects, *Perth: Curtin University of Technology. B. Sc. (Geophysics) Honor thesis,* (2010).

Calcagno, P., Chilès, J. P., Courrioux, G., and Guillen, A.: Geological modelling from field data and geological knowledge: Part I. Modelling method coupling 3D potential-field interpolation and geological rules. *Physics of the Earth and Planetary Interiors*, *171*(1), 147-157, (2008).

Corbel, S., Schilling, O., Horowitz, F. G., Reid, L. B., Sheldon, H. A., Timms, N. E., and Wilkes, P.: Identification and geothermal influence of faults in the Perth Metropolitan Area, Australia. In *Thirty-Seventh Workshop on Geothermal Reservoir Engineering, Stanford, CA*, (2012).

Costa, A.: Permeability-porosity relationship: A reexamination of the Kozeny-Carman equation based on a fractal pore-space geometry assumption. *Geophysical research letters*, *33*(2), (2006).

Crostella, A., and Backhouse, J.: *Geology and petroleum exploration of the central and southern Perth Basin, Western Australia* (No. 57). Geological Survey of Western Australia, (2000).

CSIRO: Pressure plot. Accessed 5 July 2013 at http://www.pressureplot.com/ (2007).

GEOTHERMAL ENERGY ASSOCIATION: The Geothermal Energy Association (GEA) Salutes the World's Leading Geothermal Cities. Press release December 9, 2009.

Davidson, W. A., and Yu, X.: *Perth regional aquifer modelling system (PRAMS) model development: Hydrogeology and groundwater modelling*. Department of Water, (2008).

Delle Piane, C., Esteban, L., Timms, N. E., and Ramesh Israni, S.: Physical properties of Mesozoic sedimentary rocks from the Perth Basin, Western Australia. *Australian Journal of Earth Sciences*, *60*(6-7), 735-745, (2013).

Deutsch, C. V., and Journel, A. G.: GSLIB: Geostatistical software library and user's guide: Oxford Univ. *Press, New York*, *340*, (1998).

Ehrenberg, S. N., and Nadeau, P. H.: Sandstone vs. carbonate petroleum reservoirs: A global perspective on porosity-depth and porosity-permeability relationships. *AAPG bulletin*, *89*(4), 435-445, (2005).

HDRPL: Geothermal energy potential in selected areas of Western Australia (Perth Basin), *Hot Dry Rocks Pty Ltd.*, (2008).

Laha, B., Sensharma, K., Schiffbauer, J., and Bowman, D: Effects of Immersion on Visual Analysis of Volume Data. IEEE Transactions on Visualization and Computer Graphics, 18(4), 597-606, (2012).

Lajaunie, C., Courrioux, G., and Manuel, L.: Foliation fields and 3D cartography in geology: principles of a method based on potential interpolation. *Mathematical Geology*, *29*(4), 571-584, (1997).

Middleton, M. F.: Radiogenic heat generation in the Darling Range, Western Australia. *Exploration Geophysics*, *44*(3), 206-214, (2013).

Miederau, J.: Calibration of a Fractal Model Relating Porosity to Permeability and its Use for Modeling Hydrothermal Transport Processes in the Perth Basin, Australia. *Energy Procedia*, *59,* 293-300, (2014).

Pape, H., Clauser, C., and Iffland, J.: Permeability prediction based on fractal pore-space geometry. *Geophysics*, *64*(5), 1447-1460, (1999).

Pape, H., Clauser, C., and Iffland, J.: Variation of permeability with porosity in sandstone diagenesis interpreted with a fractal pore space model. In *Fractals and Dynamic Systems in Geoscience* (pp. 603-619). Birkhäuser Basel, (2000).

Poulet, T., and Corbel, S.: Project 1: WAGCoE data catalogue. Accessed 10 September 2013 at http://geotherm.arrc.csiro.au/final_reports/Project1%20WAGCoE%20Data%20Catalogue%20WEB.pdf (2012).

Reid, L. B., Bloomfield, G., Ricard, L. P., Botman, C., and Wilkes, P.: Shallow geothermal regime in the Perth Metropolitan Area. *Australian Journal of Earth Sciences*, *59*(7), 1033-1048, (2012a).

Reid, L. B., Corbel, S., Poulet, T., Ricar, L.P., Schilling, O., Sheldon, H.A. and Wellmann, J.F.: Project 3: Hydrothermal modelling in the Perth Basin, Western Australia. *WA Geothermal Centre of Excellence,* p. 177, (2012b).

Ricard, L., Esteban, L., Pimienta, L., Delle Piane, C., Evans, C., Chanu, J. B. and Sarout, J.: Temperature estimates for geothermal application: Cockburn 1, Perth Basin, Australia. *Australian Geothermal Energy Conference 2011*, (2011).

Ricard, L., Trefry, M., Reid, L., Corbel, S., Esteban, L., Chanu, J., Wilkes, P., Douglas, G., Kaksonen, A., Lester, D., Metcalfe, G., Pimienta, L., Gutbrodt, S., Tressler, S., Bloom_eld, G., Evans, C., and Regenauer-Lieb, K.: Project 4: Productivity and sustainability of low-temperature geothermal resources, *WA Geothermal Centre of Excellence*, p. 123, (2012).

Schilling, O., Sheldon, H. A., Reid, L. B., and Corbel, S.: Hydrothermal models of the Perth metropolitan area, Western Australia: implications for geothermal energy. *Hydrogeology Journal*, *21*(3), 605-621, (2013).

Sheldon, H. A., Reid, L. B., Florio, B., Kirkby, A. L., and Budd, A. R: Convection or conduction? Interpreting temperature data from sedimentary basins. In *Proceedings of the 2011 Australian Geothermal Energy Conference* (pp. 16-18), (2011).

Sheldon, H. A., Florio, B., Trefry, M. G., Reid, L. B., Ricard, L. P., & Ghori, K. A. R.: The potential for convection and implications for geothermal energy in the Perth Basin, Western Australia. *Hydrogeology Journal*, *20*(7), 1251-1268, (2012).

Timms, N. E., Corbel, S., Olierook, H., Wilkes, P., Delle Piane, C., Sheldon, H., Alix,r., Horowitz, F., Wilson, M., Evans, K. A., Griffiths, C., Stütenbecker, L., Israni, S., Hamilton, P.J., Esteban, L., Cope, P., Evans, C., Pimienta, L., Dyt, C., Huang, X., Hopkins, J. and Champion, D.: Project 2: Geomodel. *WA Geothermal Centre of Excellence*, p. 188, (2012).